

## THE IMPORTANCE OF NEBULAR CONTINUUM AND LINE EMISSION IN OBSERVATIONS OF YOUNG MASSIVE STAR CLUSTERS

AMY E. REINES, DAVID L. NIDEVER, DAVID G. WHELAN AND KELSEY E. JOHNSON<sup>\*</sup>  
Department of Astronomy, University of Virginia, P.O. Box 400325, Charlottesville, VA 22904-4325

*Draft version October 23, 2018*

### ABSTRACT

In this spectroscopic study of infant massive star clusters, we find that continuum emission from ionized gas rivals the stellar luminosity at optical wavelengths. In addition, we find that nebular line emission is significant in many commonly used broad-band *Hubble Space Telescope* (*HST*) filters including the F814W *I*-band, the F555W *V*-band and the F435W *B*-band. Two young massive clusters (YMCs) in the nearby starburst galaxy NGC 4449 were targeted for follow-up spectroscopic observations after Reines et al. (2008a) discovered an F814W *I*-band excess in their photometric study of radio-detected clusters in the galaxy. The spectra were obtained with the Dual Imaging Spectrograph (DIS) on the 3.5 m Apache Point Observatory (APO) telescope<sup>1</sup> and have a spectral range of  $\sim 3800\text{--}9800$  Å. We supplement these data with *HST* and Sloan Digital Sky Survey (SDSS) photometry of the clusters. By comparing our data to the Starburst99 and GALEV evolutionary synthesis models, we find that nebular continuum emission competes with the stellar light in our observations and that the relative contribution from the nebular continuum is largest in the *U*- and *I*-bands, where the Balmer (3646 Å) and Paschen jumps (8207 Å) are located. The spectra also exhibit strong line emission including the [S III]  $\lambda\lambda 9069, 9532$  lines in the *HST* F814W *I*-band. We find that the *combination* of nebular continuum and line emission can account for the F814W *I*-band excess previously found by Reines et al. (2008a). In an effort to provide a benchmark for estimating the impact of ionized gas emission on photometric observations of young massive stellar populations, we compute the relative contributions of the stellar continuum, nebular continuum, and emission lines to the total observed flux of a 3 Myr-old cluster through various *HST* filter/instrument combinations, including filters in the Wide Field Camera 3 (WFC3). We urge caution when comparing observations of YMCs to evolutionary synthesis models since nebular continuum and line emission can have a large impact on magnitudes and colors of young ( $\lesssim 5$  Myr) clusters, significantly affecting inferred properties such as ages, masses and extinctions.

*Subject headings:* galaxies: individual (NGC 4449) — galaxies: starburst — galaxies: star clusters — H II regions — ISM: lines and bands

### 1. INTRODUCTION

Massive star clusters are an important mode of star formation, having an impact on a wide range of galaxy properties. However, the earliest stages of these clusters are notoriously challenging to study since the youngest clusters are still enshrouded in remnants of their gaseous and dusty birth cocoons. Properly accounting for the effects of gas and dust on observations of young massive clusters (YMCs) is nontrivial, rendering it difficult to understand their formation and earliest phases of evolution. Some of these difficulties, such as interstellar extinction, are commonly dealt with in studies of young star clusters. While it is often not possible to completely disentangle the effects of extinction, the general effects are well-known and accounted for (e.g. Calzetti et al. 1994; Whitmore et al. 1999; Johnson et al. 1999; Reines et al. 2008b).

On the other hand, the treatment of ionized gas emission can be quite complicated and the effects of nebular emission on broad-band observations of YMCs are

not always obvious. Emission lines detected via spectroscopy or narrow-band imaging, however, have proved useful for both identifying young ( $\lesssim 10$  Myr) clusters (e.g. H $\alpha$ ) and serving as valuable diagnostics on their physical conditions (e.g. Eissner et al. 1969; Castaneda et al. 1992; Kewley & Dopita 2002). If these lines are strong enough, as is typically the case for massive star forming regions, the composite emission can even affect the integrated broad-band photometry (e.g. Johnson et al. 1999; Anders & Fritze-v. Alvensleben 2003). However, nebular emission also takes on a more subtle form via continuum emission (e.g. free-free, free-bound). In fact, discontinuities or “jumps” in the nebular continuum (e.g. the Balmer and Paschen jumps) can be strong enough to serve as diagnostics in their own right (see Guseva et al. 2006, and references therein). This nebular continuum emission can also severely affect the broad-band photometry of very young clusters (e.g. Leitherer & Heckman 1995; Mollá et al. 2009).

In this paper we investigate the impact of nebular continuum and line emission on observations of very young massive star clusters. We carry out a detailed multi-wavelength study of two YMCs that are still partially embedded in their birth material. The clusters were targeted for spectroscopic follow-up after Reines et al. (2008a) found an *HST* F814W *I*-band excess in their pho-

Electronic address: areines@virginia.edu

<sup>\*</sup> Adjunct at National Radio Astronomy Observatory, 520 Edgemont Road, Charlottesville, VA 22903, USA

<sup>1</sup>The 3.5 m Apache Point Observatory telescope is owned and operated by the Astrophysical Research Consortium.

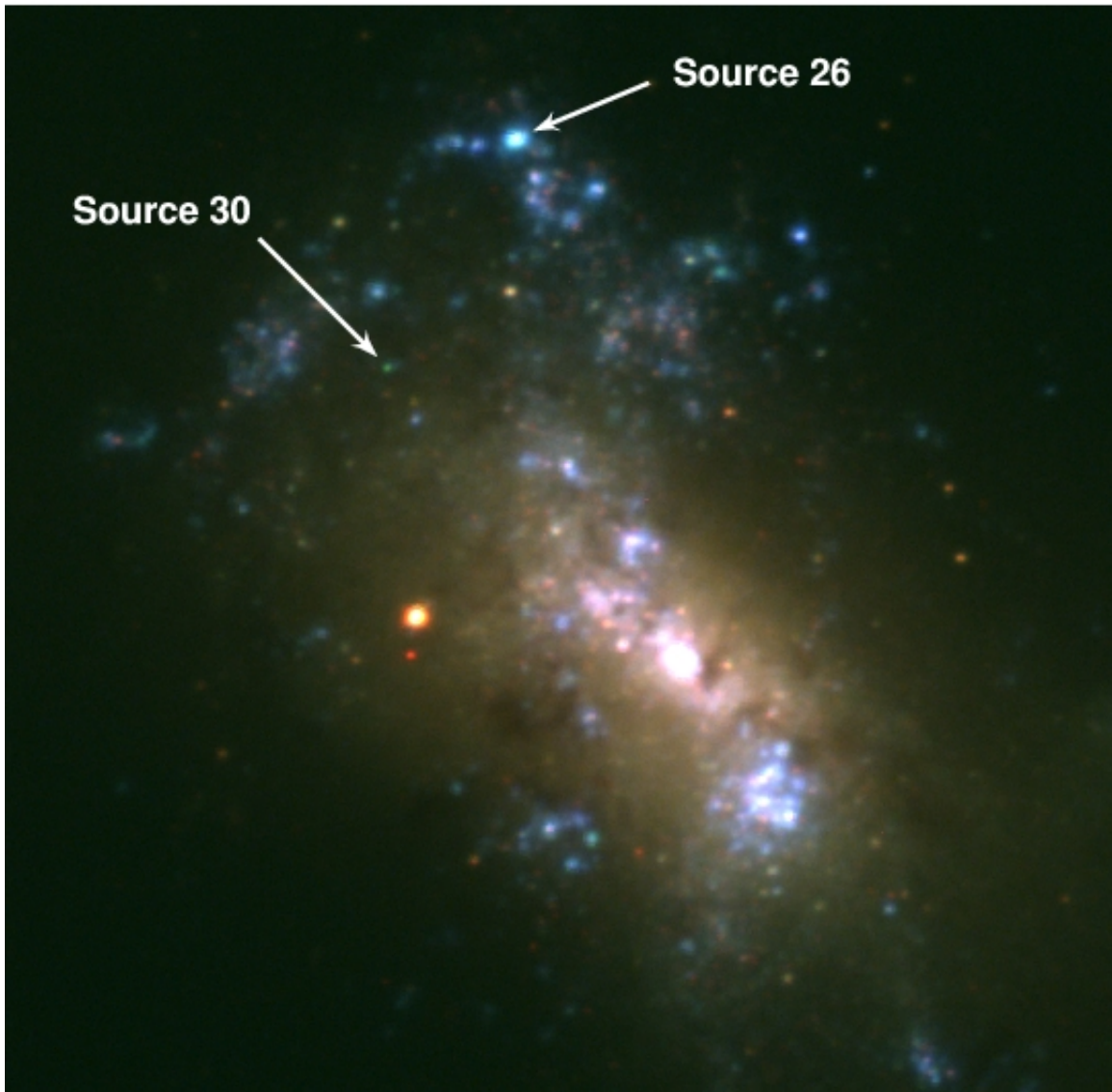


FIG. 1.— An SDSS 3-color image of NGC 4449 (RGB= $ugi$ ) using a logarithmic scaling. The two YMCs for which we have spectra are labeled (Sources 26 and 30 according to the notation of Reines et al. 2008a). The field of view is approximately  $3' \times 3'$ .

tometric study of radio-detected clusters in the nearby dwarf starburst galaxy NGC 4449. Reines et al. (2008a) considered several possible explanations for this  $I$ -band excess, including red supergiants, emission lines, thermal emission from hot dust, continuum emission from a sub-population of deeply embedded stars, and Extended Red Emission (ERE; Witt & Vijn 2004). With the observations presented here, we have determined that the *combination* of nebular continuum and line emission can account for the  $I$ -band excess found by Reines et al. (2008a). Consequently, the chief goal of this study is to gain a better empirical understanding of the effects of nebular emission (both continuum and line) associated with extremely young massive star clusters.

This paper is organized as follows: The data are described in §2. In §3 we estimate the physical properties of the clusters from their  $H\alpha$  emission. We model the spectral energy distributions (SEDs) in §4 and investigate the impact of nebular emission (line and continuum) on broad-band photometry in §5. A summary of our main

conclusions is given in §6.

## 2. DATA

A three-color SDSS image of NGC 4449 is shown in Figure 1 with our target YMCs labeled. Source 26 (according to the notation of Reines et al. 2008a) was selected for its brightness (to get a high signal-to-noise spectrum) and Source 30 was targeted for its large  $I$ -band excess – the largest of all of the clusters studied in Reines et al. (2008a). We adopt a distance of 3.9 Mpc to NGC 4449 as in Reines et al. (2008a), consistent with the results of Annibali et al. (2008). At this distance,  $1'' \sim 19$  pc.

### 2.1. Spectroscopy

Spectra of the two YMCs were obtained using the 3.5 m APO telescope. Source 26 (RA =  $12^{\text{h}} 28^{\text{m}} 13.86^{\text{s}}$ , DEC =  $+44^{\circ} 07' 10.4''$ ) was observed on the night of 2008 April 13 under clear conditions and Source 30 (RA =  $12^{\text{h}} 28^{\text{m}} 16.02^{\text{s}}$ , DEC =  $+44^{\circ} 06' 29.3''$ ) was observed on 2009



TABLE 1  
ARCHIVAL *HST* OBSERVATIONS OF NGC 4449

Filter	Instrument	Description	Exp. Time (s)	Proposal ID	PI
F170W	WFPC2	UV	400 × 2	6716	T. Stecher
F336W	WFPC2	WFPC2 U	260 × 2	6716	T. Stecher
F435W	ACS/WFC	Johnson B	3660	10585	A. Aloisi
F550M	ACS/WFC	Narrow V	1200	10522	D. Calzetti
F658N	ACS/WFC	H $\alpha$ + [NII] $\lambda$ 6584	1539	10585	A. Aloisi
F660N	ACS/WFC	[NII] $\lambda$ 6584	1860	10522	D. Calzetti
F814W	ACS/WFC	Broad I	2060	10585	A. Aloisi

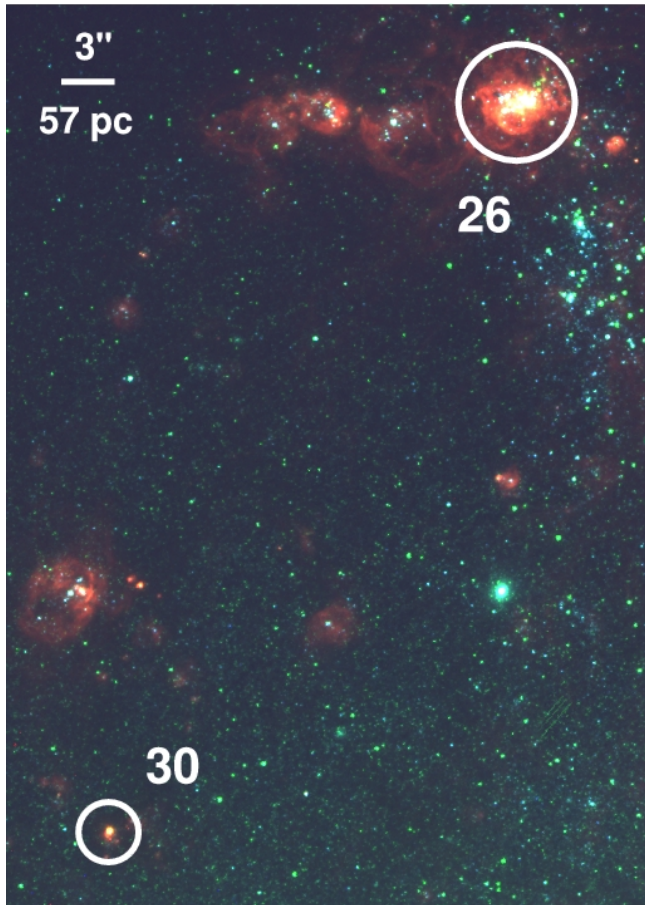


FIG. 3.— An *HST* 3-color image of NGC 4449 in the vicinity of Sources 26 and 30. Red, green and blue correspond to the F658N (H $\alpha$ ), F814W (broad *I*), and F550M (narrow *V*) filters. The circles indicate the photometric apertures used on the *HST* and SDSS imaging (see §2.2).

et al. (2008a) and summarized in Table 1. Here we use WFPC2 F170W and F336W images, as well as ACS Wide Field Channel (WFC) images through the F435W, F550M, F658N, F660N and F814W filters. The broad-band filters (F170W, F336W, F435W, F550M and F814W) span ultraviolet through near-IR wavelengths. The narrow-band filters, F658N and F660N, capture H $\alpha$  + [N II]  $\lambda$ 6584 and [N II]  $\lambda$ 6584 emission, respectively. We have also obtained *ugriz* imaging of NGC 4449 from the SDSS Data Release 6 (York et al. 2000; Adelman-McCarthy et al. 2008). A three-color (RGB=*ugi*) image of the galaxy is shown in Figure 1 with our target YMCs labeled.

Photometry of the YMCs was performed using SUR-

TABLE 2  
FLUX DENSITIES OF THE YMCs

Filter	$\lambda$ (Å)	Source 26	Source 30
<i>HST</i>			
F170W	1821	$1.3(0.1) \times 10^{-14}$	$2.2(0.7) \times 10^{-16}$
F336W	3359	$4.1(0.4) \times 10^{-15}$	$1.4(0.1) \times 10^{-16}$
F435W	4317	$2.2(0.2) \times 10^{-15}$	$7.8(0.8) \times 10^{-17}$
F550M	5581	$9.2(0.9) \times 10^{-16}$	$3.0(0.3) \times 10^{-17}$
F658N	6584	$1.6(0.2) \times 10^{-14}$	$1.1(0.1) \times 10^{-15}$
F660N	6599	$3.4(0.3) \times 10^{-15}$	$2.6(0.3) \times 10^{-16}$
F814W	8061	$5.4(0.5) \times 10^{-16}$	$3.0(0.3) \times 10^{-17}$
SDSS			
<i>u</i>	3543	$4.3(0.4) \times 10^{-15}$	$1.2(0.1) \times 10^{-16}$
<i>g</i>	4770	$3.0(0.3) \times 10^{-15}$	$1.6(0.2) \times 10^{-16}$
<i>r</i>	6231	$1.8(0.2) \times 10^{-15}$	$8.3(0.9) \times 10^{-17}$
<i>i</i>	7625	$4.9(0.5) \times 10^{-16}$	$1.8(0.2) \times 10^{-17}$
<i>z</i>	9134	$4.0(0.4) \times 10^{-16}$	$1.7(0.3) \times 10^{-17}$

NOTE. — Units of flux density are  $\text{erg s}^{-1} \text{cm}^{-2} \text{Å}^{-1}$ . Uncertainties are shown in parentheses.

PHOT (Reines et al. 2008a), a custom IDL program allowing for consistent apertures and background annuli across multiple wavebands. Circular apertures of radii  $3''3$  and  $1''7$  were used for Sources 26 and 30, respectively. Background levels were determined in annuli with inner and outer radii equal to  $1.75\times$  and  $2.5\times$  the aperture radii. Aperture sizes were chosen to include essentially all of the light from the clusters in all bands, and were mostly influenced by the (seeing-limited) resolution of the ground-based SDSS images and the intrinsic cluster sizes. Figure 3 shows a three-color *HST* image of the clusters with the photometric apertures overlaid. Flux densities for the YMCs are given in Table 2 and plotted in Figure 2 along with the spectra.

### 2.3. A Comparison of the Spectroscopic and Photometric Data

#### 2.3.1. Broad-band Flux Densities

In order to compare our spectroscopic observations with the broad-band imaging data, we simulate “DIS photometry” by convolving the YMC spectra with the total system throughput curves for the *g*, F550M, *r*, *i*, and F814W filters.<sup>3</sup> Figure 4 shows the broad-band flux densities obtained from the imaging data (listed in Table 2), as well as the flux densities obtained from the

<sup>3</sup> The observed spectra do not cover the entire wavelength ranges of the F435W and *z* filters.

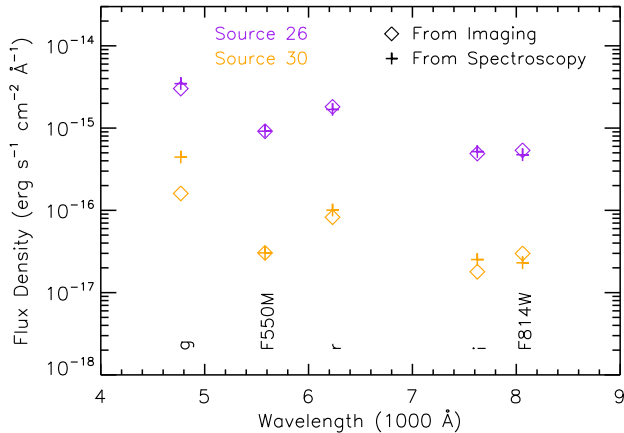


FIG. 4.— Broad-band flux densities obtained from the imaging data (diamonds) and from convolving the observed spectra with the total system throughput curves for the filters shown (plus signs). The sizes of the plot symbols reflect the errors. The spectroscopic data has been scaled to match the F550M photometry to account for loss of light in the slit. The discrepancy between the  $g$  flux densities for Source 30 are most likely due to an incorrect absolute flux level in the blue part of the spectrum (see §2.3.1).

spectroscopy.

Figure 4 illustrates that the flux densities obtained from convolving the spectra with the filter throughput curves match the the photometry quite well, especially for Source 26 which has a high signal-to-noise spectrum. However, the SDSS  $g$  flux densities for Source 30 are clearly discrepant, with the spectroscopic value significantly higher than the photometric value. We believe this is due to an incorrect absolute flux level in the blue part of the spectrum for two reasons. First, we expect the F435W photometric data point to lie above the continuum in Figure 2 since this filter contains strong emission lines (e.g.  $H\gamma$  and  $H\delta$ ). This effect can be seen for Source 26 in Figure 2 (i.e. the F435W data point lies above the continuum in the spectrum), and the emission lines are even stronger relative to the continuum for Source 30. The second reason we think the blue end of the spectrum of Source 30 has an incorrect flux level is that no single model SED can reproduce the shape of the continuum in the spectrum. There is no combination of age and extinction that can simultaneously produce such a steep blue spectrum and flattened red spectrum. Also, we show later in §4 that the best-fitting SED to the broad-band photometric data has a much flatter slope than the blue part of the spectrum of Source 30.

It is not absolutely clear why the spectrum of Source 30 has an incorrect absolute flux level in the blue, although it is most likely due to the bad weather (clouds) during the observations. We note that besides the  $g$ -band, the flux densities derived from the spectroscopy are consistent with the *HST* and SDSS photometry, and that the error in the absolute flux level in the blue part of the spectrum of Source 30 does not affect our analysis or conclusions.

### 2.3.2. $H\alpha$ Emission

In studies of extragalactic massive star forming regions, narrow-band imaging is commonly used to estimate the emission of  $H\alpha$ , which in turn is used to infer physi-

cal properties such as ionizing luminosity, age and mass. Since we have spectroscopy and narrow-band imaging of our target clusters, we compare the flux and equivalent width of  $H\alpha$  from both data sets to see how well the measurements agree.

Using the *HST* photometry, the  $H\alpha$  flux,  $F_{H\alpha}$ , and equivalent width,  $W_{H\alpha}$ , are given by

$$F_{H\alpha} = \left[ \left( f_{F658N} - f_{\text{cont}}^{(H\alpha)} \right) \Delta\lambda_{F658N} \right] - \left[ \left( f_{F660N} - f_{\text{cont}}^{(NII)} \right) \Delta\lambda_{F660N} \right], \quad (1)$$

and

$$W_{H\alpha} = \frac{F_{H\alpha}}{f_{\text{cont}}^{(H\alpha)}}, \quad (2)$$

where  $F_{H\alpha}$  has units of  $\text{erg s}^{-1} \text{cm}^{-2}$ ,  $W_{H\alpha}$  has units of  $\text{\AA}$  and  $f_{\text{cont}}^{(H\alpha)}$  is the continuum flux density at 6563  $\text{\AA}$  in  $\text{erg s}^{-1} \text{cm}^{-2} \text{\AA}^{-1}$ .

In Equation 1, the first term in square brackets is the total  $H\alpha + [N II] \lambda 6584$  flux and the second term in square brackets is the total  $[N II] \lambda 6584$  flux.<sup>4</sup> The measured flux densities and widths of the F658N and F660N filters are given by  $f_{F658N}$ ,  $f_{F660N}$  and  $\Delta\lambda_{F658N}$ ,  $\Delta\lambda_{F660N}$ , respectively. The flux densities of the continuum values,  $f_{\text{cont}}^{(H\alpha)}$  and  $f_{\text{cont}}^{(NII)}$ , are found by interpolating between the F550M and  $i$ -band data points.

Table 3 lists the measured  $H\alpha$  fluxes and equivalent widths obtained from the photometry and from direct measurements of the  $H\alpha$  line in the spectra using the IRAF task `splot`. These values agree within the errors, confirming that the appropriate imaging data can be used to obtain reliable  $H\alpha$  measurements.

Table 3 also lists extinction corrected  $H\alpha$  fluxes using internal extinctions of  $A_V=0.4$  for Source 26 and  $A_V=0.5$  for Source 30 (see §4.1). Galactic foreground extinction is also accounted for ( $E(B-V) = 0.019$ , Schlegel et al. 1998). A comparison of the  $H\alpha$  measurements with radio continuum observations (Reines et al. 2008a) suggest that these  $A_V$  may actually underestimate the true extinctions of these infant clusters since optical observations may not probe the deepest embedded regions of the YMCs. Nonetheless, we use the optically derived extinctions here.

## 3. PHYSICAL PROPERTIES OF THE CLUSTERS DERIVED FROM $H\alpha$ EMISSION

### 3.1. Ionizing Luminosities

The flux and equivalent width of the  $H\alpha$  emission line can be used to infer properties of a YMC such as the number of ionizing photons produced by the massive stars, the cluster's age, and its mass (e.g. Alonso-Herrero et al. 1996; Reines et al. 2008b). We calculate ionizing luminosities,  $N_{\text{Lyc}}$ , using the extinction corrected  $H\alpha$  luminosities (Table 3) in the following equation derived from Condon (1992) for a  $10^4$  K gas:

$$\left( \frac{N_{\text{Lyc}}}{\text{s}^{-1}} \right) \gtrsim 7.87 \times 10^{11} \left( \frac{L_{H\alpha}}{\text{erg s}^{-1}} \right). \quad (3)$$

<sup>4</sup> The  $[N II]$  line at 6548  $\text{\AA}$  is a relatively weak contaminant to the  $H\alpha$  flux and the filter throughput drops at this wavelength.

TABLE 3  
H $\alpha$  EMISSION AND DERIVED PROPERTIES OF THE YMCs

	Observed Flux (erg s $^{-1}$ cm $^{-2}$ )	Extinction Corrected Flux (erg s $^{-1}$ cm $^{-2}$ )	Equivalent Width ( $\text{\AA}$ )	N $_{\text{Ly}\alpha}$ (10 $^{49}$ s $^{-1}$ )	Age (Myr)	Mass (10 $^3$ M $_{\odot}$ )
Source 26						
Photometry	1.1(0.1) $\times 10^{-12}$	1.6(0.2) $\times 10^{-12}$	1600(370)	230(40)	(0.1)2.9(0.8)	65(12)
Spectroscopy	9.5(0.3) $\times 10^{-13}$	1.4(0.1) $\times 10^{-12}$	1500(50)	200(30)	(0.1)3.0(0.1)	62(9)
Source 30						
Photometry	7.4(0.9) $\times 10^{-14}$	1.2(0.1) $\times 10^{-13}$	3160(730)	17(3)	$\lesssim$ 2.6	4(1)
Spectroscopy	7.3(0.2) $\times 10^{-14}$	1.2(0.1) $\times 10^{-13}$	3260(120)	17(3)	$\gtrsim$ 0.4	4(1)

NOTE. — Uncertainties are shown in parentheses.

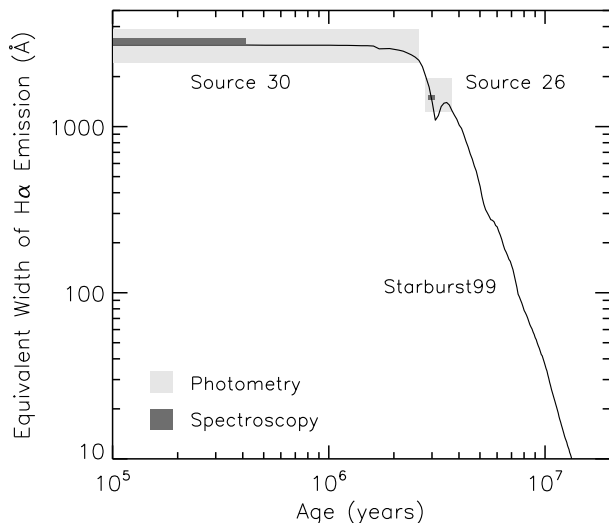


FIG. 5.— Starburst99 model evolutionary track for the equivalent width of H $\alpha$  emission (see §4.1 for a description of the model). The measured H $\alpha$  equivalent widths of Sources 26 and 30, from both the photometry and spectroscopy, are shown indicating their young ages. Uncertainties are reflected in the sizes of the shaded regions.

Adopting a distance of 3.9 Mpc to NGC 4449, the production rates of ionizing photons are approximately  $2 \times 10^{51}$  and  $1.7 \times 10^{50}$  s $^{-1}$ , or the equivalent of  $\sim 200$  and  $\sim 17$  O7.5 V stars (Vacca et al. 1996) for Sources 26 and 30, respectively. We note that the ionizing luminosity of Source 30 derived here is lower than that in Reines et al. (2008a) ( $2.7 \times 10^{50}$  s $^{-1}$ ). In that paper, the ionizing luminosity was derived from radio continuum measurements which probe higher extinction regions than the H $\alpha$  line used here.

### 3.2. Ages

Ages of the YMCs are estimated from their H $\alpha$  equivalent widths. The equivalent widths from both the photometry and spectroscopy are plotted in Figure 5 with a Starburst99 model as a function of age. We note that the model equivalent widths include a nebular component in the continuum (as do our measurements). The H $\alpha$  equivalent width of Source 26 suggests the cluster is  $\approx 3$  Myr old. Source 30 has an H $\alpha$  equivalent width consistent with the maximum value, and therefore the youngest ages, of the model evolutionary track. Source

30 is certainly younger than Source 26 and is likely  $\lesssim 1$  Myr old.

### 3.3. Masses

Assuming mass scales with ionizing luminosity, masses of the clusters can be estimated by multiplying an input model mass by the ratios of the measured ionizing luminosities to the model ionizing luminosities at their respective ages. Using the Starburst99 model described in §4.1, we infer masses of  $\sim 6 \times 10^4$  and  $\sim 4 \times 10^3$  M $_{\odot}$  for Sources 26 and 30, respectively. Again, the mass of Source 30 is lower than that presented in Reines et al. (2008a) ( $\sim 6 \times 10^3$  M $_{\odot}$ ) which used the radio derived ionizing luminosity. Ionizing luminosities, ages, and masses of Sources 26 and 30, based on the H $\alpha$  measurements presented in §2.3.2, are summarized in Table 3. It is noted that caution must be applied when interpreting the physical properties of observed clusters derived from population synthesis models, since an underlying assumption of every Simple Stellar Population (SSP) model is a well-populated Initial Mass Function (IMF) and stochastic fluctuations can bias the results.

## 4. MODELING THE STARBURST SPECTRAL ENERGY DISTRIBUTIONS

In addition to using hydrogen recombination lines such as H $\alpha$ , broad-band photometric observations of extragalactic massive star clusters are commonly compared to models of SSPs in order to estimate their physical properties such as age, extinction and mass. Here we perform SED fitting to our *photometric* data using the Starburst99 (Leitherer et al. 1999) and GALEV (Kotulla et al. 2009) evolutionary synthesis models, and investigate how well the model SEDs fit the continua in our observed *spectra*. In addition to the stellar light, both sets of models include nebular continuum (although these are computed in slightly different ways). The GALEV models also have the option to include a set of metallicity-dependent emission lines (Anders & Fritzev. Alvensleben 2003).

Physical properties of the clusters are estimated by comparing a grid of model SEDs (Starburst99 and GALEV separately) to measured photometric flux densities. The grid includes SEDs with ages  $< 50$  Myr in steps of 0.1 Myr, and visual extinctions  $< 3$  in increments of 0.1 magnitudes. We apply a 30 Doradus extinction curve adopted from Misselt et al. (1999, Table 3) and Fitzpatrick (1985, Table 6), using the parameterization given by Fitzpatrick & Massa (1990). Galactic fore-

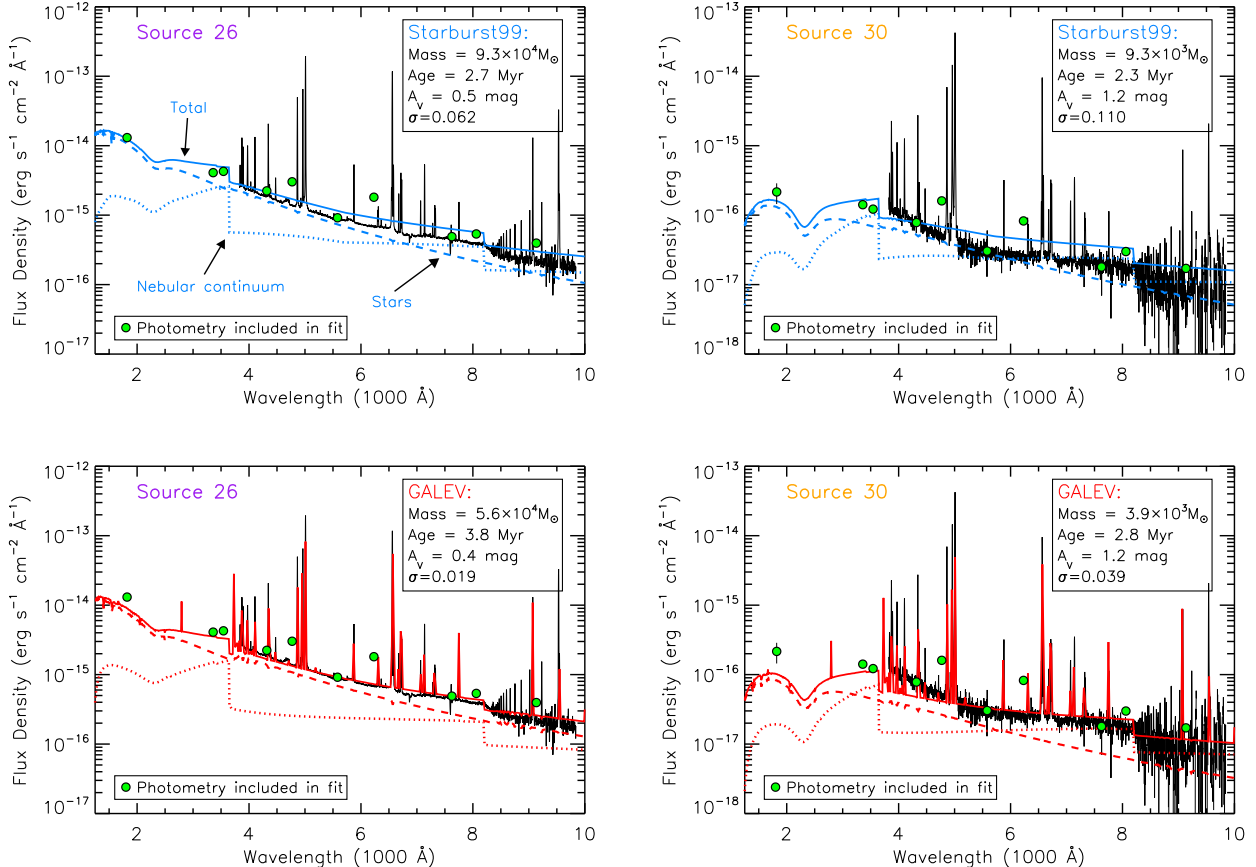


FIG. 6.— Best-fitting Starburst99 (top) and GALEV (bottom) model SEDs for Sources 26 (left) and 30 (right) using all of the photometric bands (green dots) in the fitting process. Both models include stellar continuum (dashed lines) and nebular continuum (dotted lines). The GALEV models also include emission lines. Model parameters (masses, ages and extinctions) are shown in the upper right corners of the plots. The goodness-of-fit parameter,  $\sigma$ , is also shown for each model. A lower value of  $\sigma$  indicates a better fit.

ground extinction towards NGC 4449 is also accounted for ( $E(B-V) = 0.019$ , Schlegel et al. 1998) using the extinction curve of Cardelli et al. (1989). Each model SED, of a given age and  $A_V$ , is then convolved with the total system throughput curves for the photometric filters to obtain synthetic flux densities. The best-fit model SED is determined by minimizing a goodness-of-fit parameter,  $\sigma$ , equal to the standard deviation of the logarithmic residuals of the observed and synthetic flux densities (weighted by the errors of the observed flux densities). A mass estimate is obtained by scaling the model mass by the mean logarithmic offset between the observed and best-fit model flux densities.

In all, we ran our SED fitting routine four times for each cluster: 1) using Starburst99 and all available broad-band photometric data, 2) using Starburst99 and only photometric data with minimal line emission, 3) using GALEV (with emission lines) and all available photometric data, and 4) using GALEV (without emission lines) and only photometric data with minimal line emission. Stellar and nebular continuum emission is included in the models for each case. Filters with minimal line emission were identified using our Figure 2 and Table 1 in Anders & Fritze-v. Alvensleben (2003) (for the short-wavelength filters not covered by our spectra). These include the F170W, F336W,  $u$ , F550M, and  $i$  filters. De-

tails about the models and the results of SED fitting are described below.

#### 4.1. Starburst99: Stellar and Nebular Continuum

We use the latest Starburst99 models (Version 5.1) with a metallicity of  $Z = 0.004$  (as appropriate for NGC 4449, Lequeux et al. 1979), an instantaneous burst of  $10^4 M_\odot$  with a Kroupa IMF (0.1 – 100  $M_\odot$ ), the Geneva evolutionary tracks with high mass loss, and the Pauldrach/Hillier atmospheres. The models include stellar and nebular continuum but no emission lines.

SED fitting is first performed using all of the available broad-band photometric data in this study (F170W, F336W,  $u$ , F435W,  $g$ , F550M,  $r$ ,  $i$ , F814W, and  $z$ ). The best-fitting model SEDs for Sources 26 and 30 are shown at the top of Figure 6. It is clear that the model SEDs do a poor job fitting the spectral continua. This is because the spectra contain strong emission lines which are not accounted for in the models. The photometric bands containing significant line emission cause the model SEDs to be higher than the observed continua.

Next, we perform SED fitting using only those filters with minimal line emission (F170W, F336W,  $u$ , F550M, and  $i$ ). In this case, the best-fit models do a very good job fitting both the photometry included in the fitting

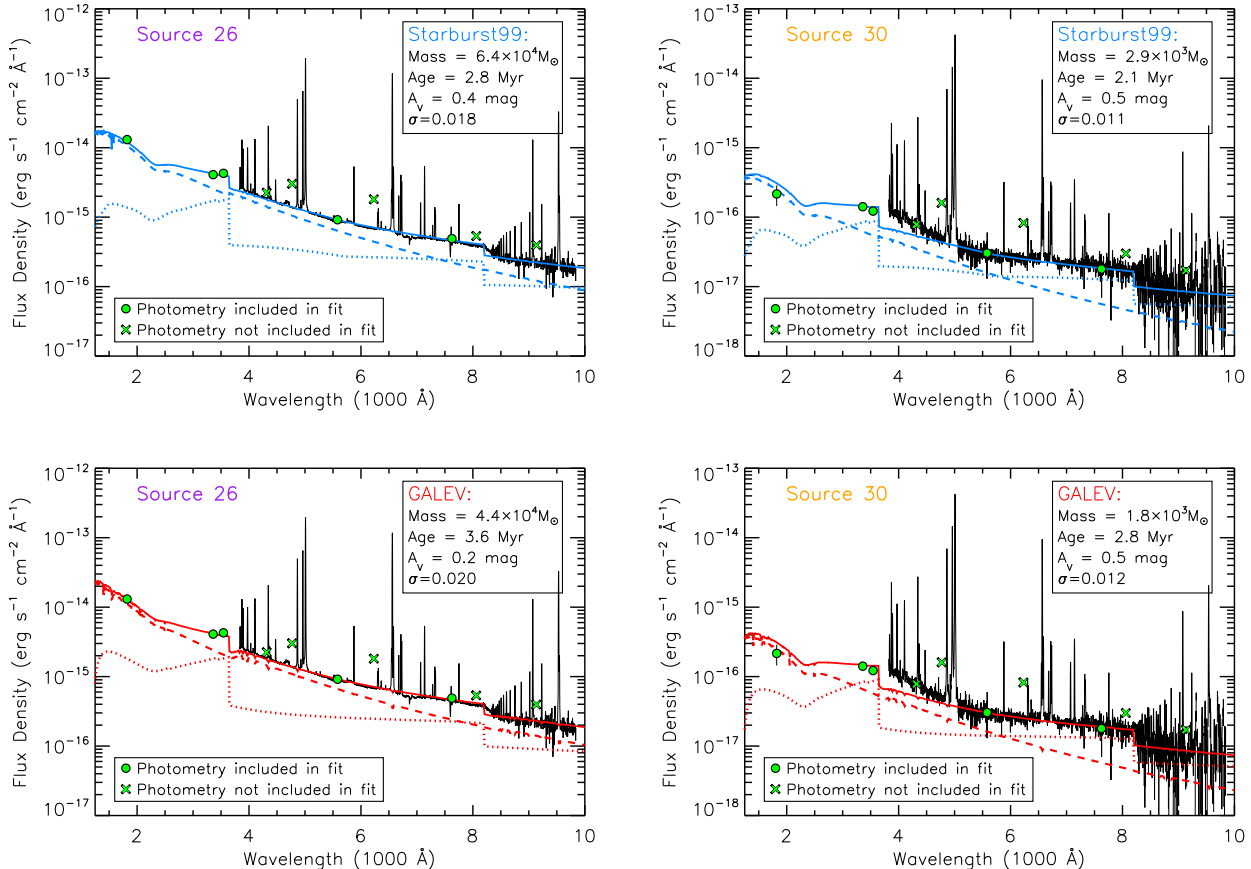


FIG. 7.— Same as Figure 6 except that only photometric bands with minimal line emission are included in the fitting process. Also, emission lines are not included in the GALEV models used here.

process and the observed continua of the spectra<sup>5</sup> (see Figure 7). Also, the inferred physical properties of the clusters (shown in Figure 7) are consistent with those derived from the  $H\alpha$  emission (see Table 3).

Comparing the best-fit Starburst99 model parameters from the two fitting processes (all bands versus bands with minimal line emission), we find that mass estimates can vary significantly. For Source 30, the mass derived from fitting all of the photometry is a factor of 3 times too high due to strong lines raising the overall SED. The extinction estimate for Source 30 is also higher by 0.7 mag when all of the bands are fit since the model SED needs to be flatter in the red to better match the F814W and  $z$ -band data (which contain significant line emission).

The impact of nebular continuum on the total SEDs is striking in both clusters (see Figure 7), especially in the  $U$ - and  $I$ -band regions of the spectra where the Balmer (3646 Å) and Paschen (8207 Å) discontinuities are located. These discontinuities, or “jumps”, in the nebular continuum emission are due to hydrogen and helium free-bound recombination processes. The nebular continuum actually dominates the total continuum in these wavelength regions for the younger YMC, Source 30.

To further illustrate the importance of nebular continuum in young stellar populations, we plot the ratio of

<sup>5</sup> The flux calibration of the blue end of the observed spectrum of Source 30 is in error (see §2.3.1). However, this does not affect our results since the photometry is being fit.

nebular continuum to the total continuum as a function of wavelength for Starburst99 model SEDs ( $Z = 0.004$ ) at various ages (Figure 8). It is clear that, at young ages, nebular continuum is a significant component of the total continuum, even at optical wavelengths.

#### 4.2. GALEV: Continuum Plus Emission Lines

GALEV models were kindly provided to us by Ralf Kotulla and the GALEV team. These models were run using the Geneva evolutionary tracks with a minimum age and time resolution of 0.1 Myr, unlike the models available on the GALEV website which use the Padova isochrones and have a minimum age and time step of 4 Myr. The models also use a “fraction of visible mass” equal to 1 rather than 0.5, which is used for the standard models available on the web (Ralf Kotulla, private communication). The models were run with a metallicity of  $Z = 0.004$  and a Kroupa IMF (0.1 – 100  $M_{\odot}$ ).

These models are very similar to the Starburst99 models described above, with the notable exception that the GALEV models include emission lines from nebular gas (Anders & Fritze-v. Alvensleben 2003; Kotulla et al. 2009). The flux of the hydrogen lines are computed using atomic physics and the production rate of ionizing photons, whereas non-hydrogen line strengths are computed using metallicity-dependent line ratios relative to  $H\beta$ . In the case of low-metallicity gas (including  $Z = 0.004$ ), observed line ratios are taken from the large sample of



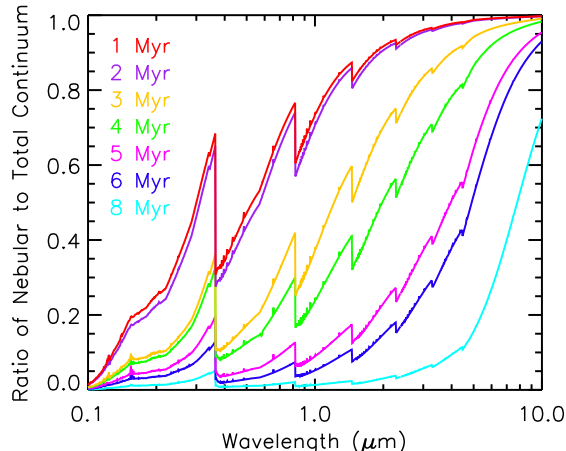


FIG. 8.— Ratio of the nebular continuum to the total continuum as a function of wavelength for a Starburst99 SSP (§4.1) at various ages. At young ages, nebular continuum is a significant component of the total continuum at optical wavelengths, especially shortward of the Balmer (3646 Å) and Paschen jumps (8207 Å) located in the  $U$ - and  $I$ -band wavelength regions. The impact of emission lines is not included here.

giant H II regions and Blue Compact Dwarf (BCD) galaxies presented in Izotov et al. (1994, 1997) and Izotov & Thuan (1998).

We perform SED fitting with the GALEV models in the same way as the Starburst99 models. First we fit all of the photometric filters and include emission lines in the models (the option to include lines is not available for Starburst99). The best-fitting model SEDs for Sources 26 and 30 are shown in Figure 6. It is clear that the GALEV models including emission lines do a much better job matching the continua in the observed spectra than the Starburst99 models do when we fit all of the photometry. However, the GALEV model SEDs shown in Figure 6 are still a bit too high in the red to near-infrared and too low in the ultraviolet. This is likely due to mismatched line intensities between the models and the observed spectra. We note that currently the GALEV models are missing the higher level Paschen lines, although they do include Pa $\alpha$  through Pa $\epsilon$ . Overall, however, the GALEV models including emission lines perform much better than the Starburst99 models when we fit all of the photometry including bands with significant line contamination.

We also only fit the photometry with minimal line emission with GALEV SEDs as we did with the Starburst99 models. Here we exclude emission lines in the models so they only contain components from the stellar and nebular continua. The best-fitting SEDs are shown in Figure 7. These models perform equally well as the Starburst99 models fit only to the photometry with minimal line emission (also shown in Figure 7). However, it is curious that the best-fit model parameters from the two families of models are as different as they are. The differences may be due to the ways in which the nebular continuum is calculated. The best-fit GALEV SEDs shown in Figure 7 also do a better job fitting the continua of the observed spectra than the GALEV models (including lines) fit to all of the photometry (Figure 6).

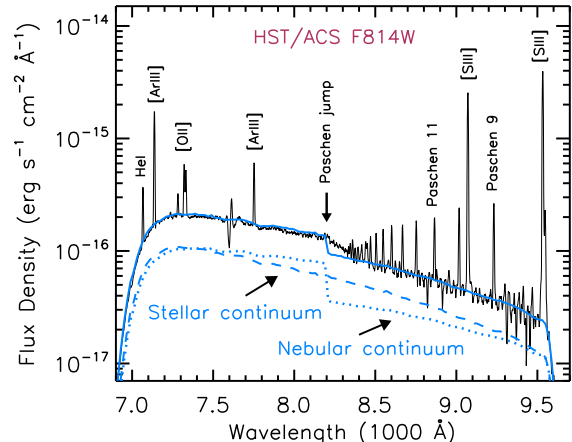


FIG. 9.— Spectrum of Source 26 multiplied by the *HST*/ACS WFC F814W total system throughput curve. The best-fitting Starburst99 model SED from Figure 7 is shown as a solid blue line. The stellar and nebular continua are shown as dashed and dotted lines, respectively. The relative contributions of the stellar continuum, nebular continuum and emission lines to the total flux of this filter are approximately 40%, 40% and 20%.

## 5. THE IMPORTANCE OF NEBULAR EMISSION IN BROAD-BAND PHOTOMETRY

A number of authors have discussed the impact of nebular emission on broad-band photometry of young stellar populations based on synthesis modeling (e.g. Krueger et al. 1995; Leitherer & Heckman 1995; Zackrisson et al. 2001; Anders & Fritze-v. Alvensleben 2003; Mollá et al. 2009). Our spectrophotometric observations of infant massive star clusters clearly support the conclusion that nebular emission, both in lines and continuum, significantly affects broad-band photometry of these objects.

### 5.1. Contributions to Broad-band Fluxes

In an effort to provide a benchmark for estimating the impact of nebular emission on photometric observations of young massive stellar populations, we compute the relative contributions of the stellar continuum, nebular continuum, and emission lines to the total flux of Source 26 through various *HST* filter/instrument combinations (including WFC3) and the SDSS *griz* filters.<sup>6</sup> The contribution of nebular emission in the *HST*/ACS WFC F814W filter is of particular interest since, in their study of radio-detected clusters in NGC 4449, Reines et al. (2008a) found an excess in this band relative to model SEDs for a pure stellar continuum.

The spectrum of Source 26 multiplied by the *HST*/ACS WFC F814W total system throughput curve is shown in Figure 9. The best-fitting Starburst99 model SED (from Figure 7) is also shown. In addition to stellar and nebular continuum, the spectrum contains several prominent emission lines in this band. The strongest are [S III]  $\lambda$ 9532 and [S III]  $\lambda$ 9069. A number of other lines, including the Paschen series, are detected and labeled in Figure 9.

We determine the relative contributions of stellar continuum, nebular continuum and emission lines to the to-

<sup>6</sup> We do not use the spectrum of Source 30 since it has a low signal-to-noise ratio and the flux calibration is uncertain in the blue (see §2.1 and §2.3.1).

TABLE 4  
RELATIVE CONTRIBUTIONS TO BROAD-BAND FLUXES OF SOURCE 26

Filter	Instrument	Stellar Continuum	Nebular Continuum	Emission Lines
<i>HST</i> Medium and Wide Filters in the <i>I</i> -band Region				
F845M	WFC3/UVIS	0.49	0.41	0.09
F814W	WFC3/UVIS	0.39	0.38	0.23
F814W	ACS/WFC	0.41	0.39	0.20
F814W	ACS/HRC	0.38	0.36	0.25
F814W	WFPC2	0.41	0.40	0.20
F791W	WFPC2	0.46	0.45	0.10
F775W	WFC3/UVIS	0.46	0.45	0.09
F775W	ACS/WFC	0.46	0.46	0.08
F775W	ACS/HRC	0.46	0.46	0.08
F763M	WFC3/UVIS	0.47	0.50	0.03
<i>HST</i> Medium and Wide Filters in the <i>V</i> -band Region				
F555W	WFC3/UVIS	0.31	0.12	0.56
F555W	ACS/WFC	0.27	0.11	0.63
F555W	ACS/HRC	0.26	0.11	0.63
F555W	WFPC2	0.32	0.13	0.54
F550M	ACS/WFC	0.70	0.31	0.00
F550M	ACS/HRC	0.70	0.31	0.00
F547M	WFC3/UVIS	0.71	0.30	0.00
F547M	WFPC2	0.68	0.29	0.03
SDSS Filters				
<i>g</i>	SDSS	0.32	0.10	0.58
<i>r</i>	SDSS	0.27	0.16	0.57
<i>i</i>	SDSS	0.46	0.46	0.07
<i>z</i>	SDSS	0.34	0.26	0.40

tal observed flux in the F814W filter as follows. The contributions from the stellar and nebular continua are estimated by multiplying the models for these components with the filter throughput curve and integrating over the bandpass. The total flux from emission lines in this filter is determined by multiplying the observed spectrum with the F814W filter throughput curve and measuring the flux of each line in the resulting spectrum. The relative contributions of each component are found by dividing by the total observed flux in the F814W filter (obtained by convolving the observed spectrum with the throughput curve). We find that the relative contributions of the stellar continuum, nebular continuum and emission lines to the total observed flux of Source 26 through the F814W filter are approximately 40%, 40%, and 20%, respectively. *Clearly, nebular emission contributes a significant fraction ( $\sim 60\%$ ) of the total flux in the F814W filter and should not be neglected.* The combination of nebular continuum and emission lines can account for the F814W *I*-band excess found by Reines et al. (2008a). This result is consistent with their prediction that the origin of the excess should not affect clusters older than  $\sim 5$  Myr.

Relative contributions to the total flux of Source 26 through other *HST* filter/instrument combinations are listed in Table 4. Throughput curves were obtained using SYNPHOT, the synthetic photometry package distributed by the Space Telescope Science Data Analysis System (STSDAS). The total flux and the flux of the stellar and nebular continua are found in the same way as described above. The line contributions, however, are simply estimated by subtracting the continuum contribu-

tions from the total observed flux. Plots of the observed spectrum of Source 26 multiplied by the *HST* WFC3 filters listed in Table 4 are shown in Figure 10. We find that the relative contribution of the nebular gas (continuum plus lines) to the total flux of Source 26 in any of the *HST I*-band filters listed in Table 4 is *at least 50%*. In the *V*-band, roughly 70% of the F555W flux comes from ionized gas. Younger clusters will have an even larger contribution from ionized gas. Relative contributions to the SDSS fluxes of Source 26 are also listed in Table 4 using the throughput curves available online.<sup>7</sup>

We emphasize that the quantitative results listed in Table 4 are specific to Source 26. Relative contributions will vary from source to source, depending on (at a minimum) age and metallicity (e.g. our Figure 8 and Anders & Fritze-v. Alvensleben 2003). However, it is evident that the impact of nebular emission on broad-band fluxes can be quite large and should not be readily dismissed.

## 5.2. The Impact on Magnitudes, Colors and Derived Properties

The ionized gas associated with a young stellar population can provide a significant contribution to the total observed flux in a given filter (§5.1). The nebular emission, therefore, can have large impact on the physical properties derived from magnitudes and broad-band colors.

Using the GALEV models described in Section 4.2, we have computed the magnitude difference as a function of age between a pure stellar population and one of the

<sup>7</sup> <http://www.sdss.org/dr6/instruments/imager/>

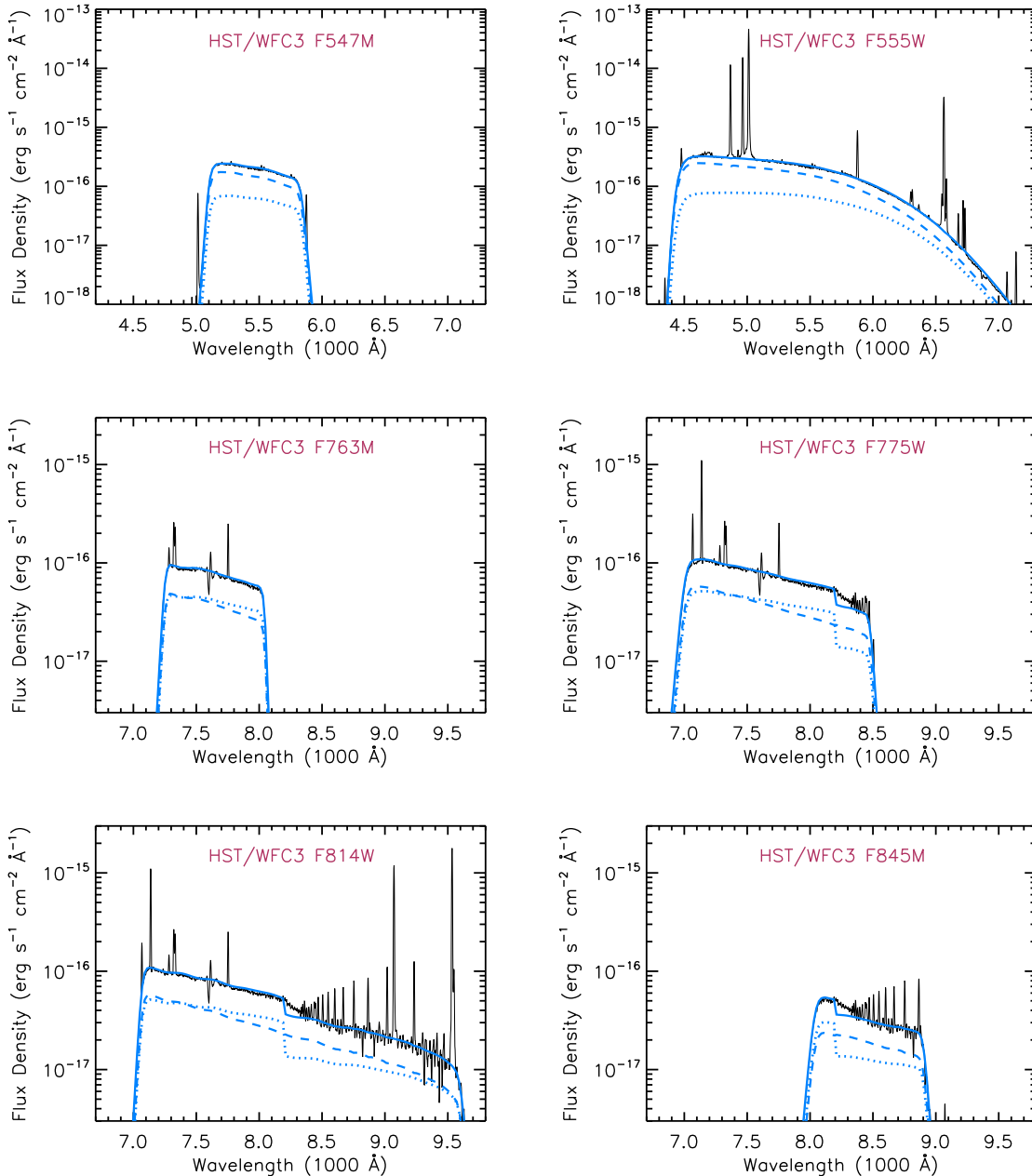


FIG. 10.— Spectrum of Source 26 multiplied by the *HST*/WFC3 filters in the *V*- and *I*-band wavelength regions listed in Table 4. The best-fitting Starburst99 model SED from Figure 7 is shown as a solid line. Individual contributions from the stellar and nebular continua are shown as dashed and dotted lines, respectively. The impact of emission lines on the flux through various filters is given in Table 4. The F555W and F814W fluxes are most affected by line emission.

same mass but including ionized gas emission (continuum plus lines) for the *HST*/WFC3 F814W (broad *I*), F555W (wide *V*), and F547M (narrow *V*) filters. The results are shown in Figure 11. For a 3 Myr old cluster, including the gaseous emission results in magnitudes that are brighter by 1.0 (F814W), 1.5 (F555W), and 0.4 (F547M) mag. Neglecting nebular emission and assuming all of the flux comes from the stars would therefore lead to overestimates of the stellar mass by factors of 2.5 (F814W), 4.0 (F555W), and 1.4 (F547M). From Figure 10, we can see that significant contributions from both nebular continuum and lines are present in the F814W filter, whereas the F555W flux is most affected by strong

lines (e.g.  $H\beta$  and  $[O\ III]$ ). The F547M flux is affected by the nebular continuum but does not contain strong line emission.

We obtain similar results from modeling the SED of Source 26 and determining the relative contributions of the stellar continuum, nebular continuum and emission lines to the total flux through various filters (§5.1). Mass (over)estimates of this YMC (age  $\approx 3$  Myr,  $Z \approx 0.004$ ), assuming all of the flux in a given filter is due only to stars, can be obtained by taking the inverse of the relative contribution of the stellar continuum to the total flux (the third column in Table 4). For example, neglecting the effects of nebular emission in the ACS/WFC F555W

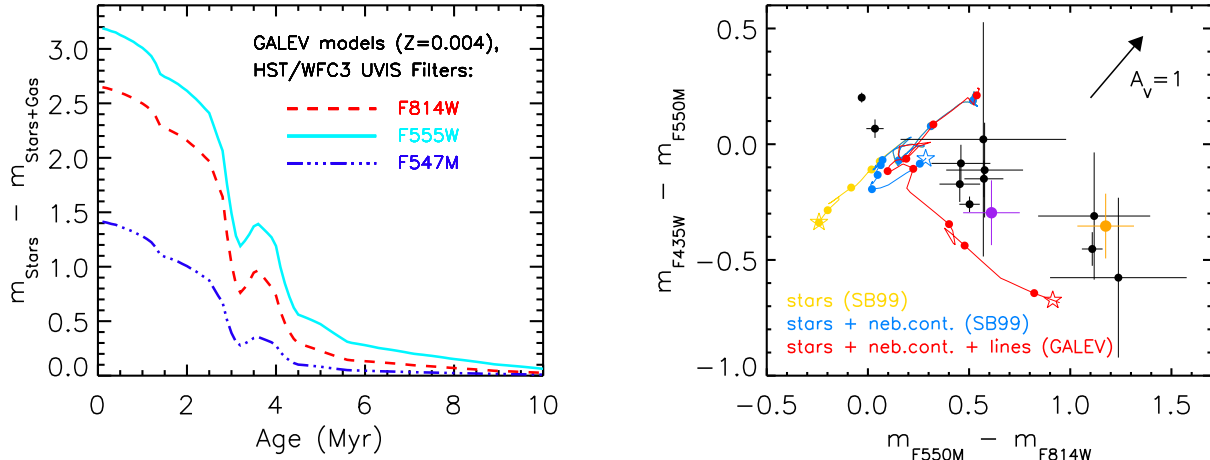


FIG. 11.— *Left*: Magnitude difference as a function of age between a pure stellar population and one of the same mass but including ionized gas emission (continuum and lines). The GALEV model SEDs described in Section 4.2 were convolved with the *HST*/WFC3 F814W (broad *I*), F555W (wide *V*), and F547M (narrow *V*) filters to produce this plot. *Right*: Color-color diagram using the *HST*/ACS WFC F435W, F550M and F814W filters and the data of Reines et al. (2008a). Sources 26 and 30 are shown as large purple and orange dots, respectively. Model evolutionary tracks are shown for a Starburst99 model with stellar continuum only (yellow), a Starburst99 model with stellar and nebular continuum (blue), and a GALEV model with stellar continuum, nebular continuum, and emission lines (red). The tracks extend to an age of 50 Myr. An age of 1 Myr is indicated by a star and the dots along the tracks indicate ages of 2, 3, 4, 5, 7, 10, 25 and 40 Myr. Observed and model colors are for the *HST* filters with VEGAMAG zeropoints.

filter would result in a mass  $3.7\times$  larger than the mass obtained by properly accounting for the gas contribution in this filter.

Since the magnitudes of young stellar populations can be considerably brightened by the presence of ionized gas, colors can also be significantly affected. For example, the work of Reines et al. (2008a) found an apparently anomalous color-color diagram in which the radio-detected YMCs in NGC 4449 with the bluest *HST*/ACS WFC [F435W–F550M] colors had the reddest [F550M–F814W] colors, contradictory to the Starburst99 model evolutionary track for a pure stellar continuum. We have reproduced this color-color diagram but have now included a Starburst99 model evolutionary track including nebular continuum, and a GALEV track including nebular continuum plus emission lines (Figure 11). Only the GALEV model is able to reproduce the trend seen in the data, signifying that emission lines have a large effect on these colors at young ages ( $\lesssim 5$  Myr). Although the F550M filter is essentially line-free, the F814W and F435W filters contain a number of emission lines. The forbidden [S III] lines at 9532 and 9069 Å are the most prominent in the F814W filter, but many others are also present (see Figure 9). The F435W filter contains line emission from H $\gamma$ , H $\delta$ , He+ [N III]  $\lambda$ 3970, H $\zeta$ + [He I]  $\lambda$ 3889, [N III]  $\lambda$ 3869, and [O II]  $\lambda$ 3727 (see our Figure 2 and Anders & Fritze-v. Alvensleben 2003).

It is worth noting that the [F435W–F550M] versus [F550M–F814W] color-color diagram may prove to be a useful diagnostic for identifying YMCs with ages  $\lesssim 5$  Myr. It is also interesting that the extinction vector in Figure 11 is perpendicular to the GALEV model track for ages  $\lesssim 5$  Myr. In other words, there is no degeneracy in this color space between age and extinction at young ages. Therefore, rough estimates of both age and extinction could be obtained from this color-color plot. However, we emphasize that the line strengths of any given

source may vary from the ones input into the GALEV models which could potentially lead to large uncertainties in the derived properties.

As a check, we look at Sources 26 and 30 (indicated in Figure 11 by purple and orange dots respectively). The ages inferred from their colors are consistent with those obtained from their H $\alpha$  equivalent widths and from SED fitting; approximately 3 Myr for Source 26 and 1-2 Myr for Source 30. The visual extinction of Source 26 also appears to be consistent with our previous estimates of  $\sim 0.4$  magnitudes. The extinction of Source 30 inferred from Figure 11 ( $\approx 1$  mag), on the other hand, is half a magnitude larger than that obtained from SED fitting to the photometry with minimal line emission (Figure 7).<sup>8</sup> This difference is likely the result of different line intensities between the models and the data. The GALEV models, however, at least qualitatively explain these colors of very young star clusters, which neither of the Starburst99 models can do.

## 6. CONCLUSIONS

This paper examines the importance of nebular continuum and line emission in observations of young massive stellar populations. We have obtained spectroscopy ( $\lambda \sim 3800 - 9800$  Å) of two young ( $\lesssim 3$  Myr) star clusters in the nearby starburst galaxy NGC 4449 and supplement these data with archival *HST* and SDSS photometry of the clusters. We compare our data to the Starburst99 and GALEV evolutionary synthesis models to estimate the physical properties of the clusters and determine the impact of ionized gas emission (line and continuum) on broad-band photometry. Our main results are summarized below:

<sup>8</sup> It is not clear that optically derived  $A_V$ 's are accurate measures of the extinction at such young ages, since a significant fraction of the cluster may be heavily embedded and visibly obscured.

1. The *combination* of nebular continuum and line emission can account for the F814W *I*-band excess found by Reines et al. (2008a) in their study of radio-detected YMCs in NGC 4449. This result is consistent with their prediction that the origin of the excess should not affect clusters older than  $\sim 5$  Myr.
2. At very young ages ( $\lesssim 3$  Myr), nebular continuum emission from ionized gas can *rival* the stellar luminosity of YMCs at optical wavelengths. The relative contribution from the nebular continuum emission is largest in the *U*- and *I*-bands, where the Balmer (3646 Å) and Paschen jumps (8207 Å) are located.
3. Nebular line emission is significant in many commonly used broad-band *HST* filters including the F814W *I*-band, the F555W *V*-band and the F435W *B*-band. Emission lines (in addition to nebular continuum) are required to explain the distribution of radio-detected YMCs in NGC 4449 in the [F435W–F550M] versus [F550M–F814W] color-color diagram first presented in Reines et al. (2008a).
4. SED fitting to broad-band photometry of YMCs is most successful when the photometric bands do not contain significant line emission. In this case, evolutionary synthesis models only containing *continuum* emission from stars and ionized gas are adequate. If the photometric bands include significant

line emission, however, models including emission lines perform much better than those that do not.

5. The impact of ionized gas emission on broad-band fluxes, magnitudes and colors can be large and should not be readily dismissed. We urge caution when comparing observations of young ( $\lesssim 5$  Myr) clusters to synthesis models since nebular continuum and line emission can significantly affect inferred properties such as ages, masses and extinctions.

We thank Ralf Kotulla for providing us with the custom-run GALEV models used in this work. We also thank the anonymous referee for numerous useful comments and suggestions which led to the overall improvement of this paper. A.E.R. appreciates helpful discussions with Adolf Witt, Yuri Izotov and Crystal Brogan. A.E.R. also gratefully acknowledges support from a NASA Earth and Space Science Fellowship, the Virginia Space Grant Consortium and the University of Virginia through a Governor's Fellowship. K.E.J. gratefully acknowledges support provided in part by NSF through CAREER award 0548103 and the David and Lucile Packard Foundation. Support for program #AR09934 was provided in part by NASA through a grant from the Space Telescope Science Institute, which is operated by the Association of Universities for Research in Astronomy, Inc., under NASA contract NAS 5-26555.

## REFERENCES

- Adelman-McCarthy, J. K., et al. 2008, *ApJS*, 175, 297  
 Aller, L. H. 1984, *Physics of Thermal Gaseous Nebulae*  
 Alonso-Herrero, A., Aragón-Salamanca, A., Zamorano, J., & Rego, M. 1996, *MNRAS*, 278, 417  
 Anders, P., & Fritze-v. Alvensleben, U. 2003, *A&A*, 401, 1063  
 Annibali, F., Aloisi, A., Mack, J., Tosi, M., van der Marel, R. P., Angeretti, L., Leitherer, C., & Sirianni, M. 2008, *AJ*, 135, 1900  
 Bohlin, R. C., Colina, L., & Finley, D. S. 1995, *AJ*, 110, 1316  
 Calzetti, D., Kinney, A. L., & Storchi-Bergmann, T. 1994, *ApJ*, 429, 582  
 Cardelli, J. A., Clayton, G. C., & Mathis, J. S. 1989, *ApJ*, 345, 245  
 Castaneda, H. O., Vilchez, J. M., & Copetti, M. V. F. 1992, *A&A*, 260, 370  
 Cerviño, M., & Luridiana, V. 2004, *A&A*, 413, 145  
 Condon, J. J. 1992, *ARA&A*, 30, 575  
 Conti, P. S. 1991, *ApJ*, 377, 115  
 Eissner, W., de A. P. Martins, P., Nussbaumer, H., Saraph, H. E., & Seaton, M. J. 1969, *MNRAS*, 146, 63  
 Fitzpatrick, E. L. 1985, *ApJ*, 299, 219  
 Fitzpatrick, E. L., & Massa, D. 1990, *ApJS*, 72, 163  
 Guseva, N. G., Izotov, Y. I., & Thuan, T. X. 2006, *ApJ*, 644, 890  
 Izotov, Y. I., Stasińska, G., Meynet, G., Guseva, N. G., & Thuan, T. X. 2006, *A&A*, 448, 955  
 Izotov, Y. I., Thuan, T. X., & Lipovetsky, V. A. 1994, *ApJ*, 435, 647  
 Izotov, Y. I., Thuan, T. X., & Lipovetsky, V. A. 1997, *ApJS*, 108, 1  
 Izotov, Y. I., & Thuan, T. X. 1998, *ApJ*, 500, 188  
 Johnson, K. E., Vacca, W. D., Leitherer, C., Conti, P. S., & Lipsky, S. J. 1999, *AJ*, 117, 1708  
 Kewley, L. J., & Dopita, M. A. 2002, *ApJS*, 142, 35  
 Kotulla, R., Fritze, U., Weilbacher, P., & Anders, P. 2009, *MNRAS*, 396, 462  
 Krueger, H., Fritze-v. Alvensleben, U., & Loose, H.-H. 1995, *A&A*, 303, 41  
 Lançon, A., & Mouhcine, M. 2000, *Massive Stellar Clusters*, 211, 34  
 Leitherer, C., et al. 1999, *ApJS*, 123, 3  
 Leitherer, C., & Heckman, T. M. 1995, *ApJS*, 96, 9  
 Lequeux, J., Peimbert, M., Rayo, J. F., Serrano, A., & Torres-Peimbert, S. 1979, *A&A*, 80, 155  
 Massey, P. 1997, *A User's Guide to CCD Reductions with IRAF*  
 Massey, P., Valdes, F., & Barnes, J. 1992, *A User's Guide to Reducing Slit Spectra with IRAF*  
 Misselt, K. A., Clayton, G. C., & Gordon, K. D. 1999, *ApJ*, 515, 128  
 Mollá, M., García-Vargas, M. L., & Bressan, A. 2009, *MNRAS*, 1016  
 Reines, A. E., Johnson, K. E., & Goss, W. M. 2008, *AJ*, 135, 2222  
 Reines, A. E., Johnson, K. E., & Hunt, L. K. 2008, *AJ*, 136, 1415  
 Schaerer, D., & Vacca, W. D. 1998, *ApJ*, 497, 618  
 Schlegel, D. J., Finkbeiner, D. P., & Davis, M. 1998, *ApJ*, 500, 525  
 Vacca, W. D., Garmany, C. D., & Shull, J. M. 1996, *ApJ*, 460, 914  
 Whitmore, B. C., Zhang, Q., Leitherer, C., Fall, S. M., Schweizer, F., & Miller, B. W. 1999, *AJ*, 118, 1551  
 Witt, A. N., & Vijh, U. P. 2004, *Astrophysics of Dust*, 309, 115  
 York, D. G., et al. 2000, *AJ*, 120, 1579  
 Zackrisson, E., Bergvall, N., Olofsson, K., & Siebert, A. 2001, *A&A*, 375, 814